Detailed balance, internal consistency, and energy conservation in fragment orbital-based surface hopping

Antoine Carof, Samuele Giannini, and Jochen Blumberger

Citation: The Journal of Chemical Physics **147**, 214113 (2017); doi: 10.1063/1.5003820
View online: https://doi.org/10.1063/1.5003820
View Table of Contents: http://aip.scitation.org/toc/jcp/147/21
Published by the American Institute of Physics

Detailed balance, internal consistency, and energy conservation in fragment orbital-based surface hopping

Antoine Carof,[1] Samuele Giannini,[1] and Jochen Blumberger[1,2,a)]
[1]*Department of Physics and Astronomy, University College London, Gower Street, London WC1E 6BT, United Kingdom*
[2]*Institute for Advanced Study, Technische Universität München, Lichtenbergstrasse 2a, D-85748 Garching, Germany*

(Received 7 September 2017; accepted 3 November 2017; published online 7 December 2017)

We have recently introduced an efficient semi-empirical non-adiabatic molecular dynamics method for the simulation of charge transfer/transport in molecules and molecular materials, denoted fragment orbital-based surface hopping (FOB-SH) [J. Spencer *et al.*, J. Chem. Phys. **145**, 064102 (2016)]. In this method, the charge carrier wavefunction is expanded in a set of charge localized, diabatic electronic states and propagated in the time-dependent potential due to classical nuclear motion. Here we derive and implement an exact expression for the non-adiabatic coupling vectors between the adiabatic electronic states in terms of nuclear gradients of the diabatic electronic states. With the non-adiabatic coupling vectors (NACVs) available, we investigate how different flavours of fewest switches surface hopping affect detailed balance, internal consistency, and total energy conservation for electron hole transfer in a molecular dimer with two electronic states. We find that FOB-SH satisfies detailed balance across a wide range of diabatic electronic coupling strengths provided that the velocities are adjusted along the direction of the NACV to satisfy total energy conservation upon a surface hop. This criterion produces the right fraction of energy-forbidden (frustrated) hops, which is essential for correct population of excited states, especially when diabatic couplings are on the order of the thermal energy or larger, as in organic semiconductors and DNA. Furthermore, we find that FOB-SH is internally consistent, that is, the electronic surface population matches the average quantum amplitudes, but only in the limit of small diabatic couplings. For large diabatic couplings, inconsistencies are observed as the decrease in excited state population due to frustrated hops is not matched by a corresponding decrease in quantum amplitudes. The derivation provided here for the NACV should be generally applicable to any electronic structure approach where the electronic Hamiltonian is constructed in a diabatic electronic state basis. *Published by AIP Publishing.* https://doi.org/10.1063/1.5003820

I. INTRODUCTION

Electronically non-adiabatic processes are of central importance in photochemistry, electron and energy transfer, proton-coupled electron transfer reactions, surface scattering, and friction, to mention just a few examples. A plethora of theoretical methods have been developed to describe non-adiabatic dynamics at a molecular scale ranging from multi-configurational time-dependent Hartree,[1,2] *ab initio* multiple spawning,[3,4] exact factorization of the molecular wavefunction,[5–7] and mixed quantum-classical non-adiabatic molecular dynamics (MQC-NAMD)[7–9] simulation such as Ehrenfest[8] and fewest switches surface hopping (FSSH) MD.[9] All these methods require the calculations of electronically excited states and excited state nuclear gradients, which makes them computationally extremely demanding when combined with *ab initio* or density functional theory-based electronic structure calculations. For certain types of non-adiabatic processes, especially those where chemical bonds remain intact, it is possible to use suitably parametrized semi-empirical electronic structure methods, e.g., self-consistent charge density functional tight binding (SCC-DFTB)[10–15] and time-dependent SCC-DFTB,[16,17] OM3,[18,19] AM1,[20,21] and Pariser-Parr-Pople (PPP) electronic Hamiltonians.[22,23] The development of reliable approaches with semi-empirical electronic structure description is particularly important for non-adiabatic processes in large systems where all parts are electronically active, thus rendering QM/MM type methods impractical or unsuitable (e.g., molecular materials).

We have recently introduced an efficient fewest switches surface hopping (FSSH) method, termed fragment orbital-based surface hopping (FOB-SH), that was tailored towards simulation of charge transport in large molecular systems.[24] In our method, the charge carrier wavefunction is expanded in the basis of fragment molecular orbitals that mediate the charge transfer. For convenience, we refer to this basis also as diabatic basis, even though it is only quasi-diabatic, i.e., the non-adiabatic couplings are not exactly zero, only rather small. Formulation of the problem in a diabatic electronic basis offers some advantages over the more common adiabatic electronic state basis favoured by most quantum chemists. For instance, it leads quite naturally to a low or even linear scaling algorithm due to the localized character of the electronic

a)Electronic mail: j.blumberger@ucl.ac.uk

states in this representation. In addition, the problem of the electron delocalisation error in DFT electronic structure calculation of adiabatic electronic states is largely suppressed. Several DFT methods are available that yield diabatic electronic states, e.g., constrained DFT,[25–29] frozen density embedding,[30,31] and DFTB.[13–15] In the context of FSSH, a drawback of diabatic states is that all energies and nuclear gradients need to be transformed to the adiabatic representation as the nuclear dynamics should be run on the adiabatic states in this method.

In our recent semi-empirical implementation of FOB-SH, explicit electronic structure calculations are only carried out for parametrization purposes, not during the propagation of the coupled electron-nuclear dynamics, which makes the method very fast. The diagonal elements of the electronic Hamiltonian (site energies) and the respective forces are calculated with a classical force field, while the off-diagonal energies (electronic couplings) and respective nuclear derivatives are obtained from the overlap of frontier orbitals.[24,32] For a detailed description of FOB-SH, we refer here to Sec. II and Ref. 24. We note in passing that our approach shares certain similarities with other semi-empirical implementations of non-adiabatic dynamics, e.g., the DFTB method of Elstner and co-workers[13,14] and the fragment molecular orbital method of Akimov.[33] Also in these approaches, the electronic Hamiltonian is directly constructed in a site or fragment basis requiring the calculation of site energies and electronic couplings. Yet, in our recent work, we went one step further by showing how the exact nuclear forces on the adiabatic electronic states can be obtained from the nuclear gradients in the diabatic representation.[24]

A first application of our methodology to electron hole transport along a chain of ethylene-like molecules reproduced the well-known crossover from activated to band-like charge transport as the diabatic electronic coupling between the molecules is increased.[24] Moreover, we could show that FOB-SH reproduces very well the dependence of the electron transfer (ET) rate in a molecular dimer with respect to reorganization energy, diabatic electronic coupling, and driving force, as predicted by the classical Marcus theory.[66] However, the decay of the ET rate and excited state population with increasing reorganization energy was underestimated. A possible reason for this was the specific energy criterion used in determining whether an attempted hop is successful or not. We used the total kinetic energy of the system rather than the kinetic energy component parallel to the non-adiabatic coupling vector (NACV) as recommended by Tully and others. We adopted this choice because NACVs between the adiabats were not available in the first version of our implementation (note, in FSSH only the non-adiabatic coupling matrix elements (NACEs) are needed for electronic propagation and calculation of hopping probabilities).

In this work, we present a rigorous derivation of the NACVs between the adiabatic electronic states in terms of nuclear gradients of the (non-orthogonal) diabatic states. The final expression comprises three terms. The first term is proportional to the nuclear gradient of the electronic Hamiltonian in the diabatic basis divided by the adiabatic energy gap. It resembles the usual expression for the NACV in the adiabatic electronic state basis and gives the largest contribution. The other two terms contain NACVs between the non-orthogonal diabatic states and the nuclear gradient of the matrix that orthogonalizes the diabatic states (here, a Löwdin transformation matrix). We show numerically that these latter two terms can be neglected.

With the NACVs available, we investigate how different prescriptions/flavours of FSSH affect detailed balance (i.e., the thermal equilibrium population of excited states),[34] internal consistency between electronic surface population and quantum amplitudes,[35] and drift of conserved energy. The model system we consider is electron hole transfer between two ethylene-like molecules with diabatic electronic coupling values spanning the non-adiabatic, adiabatic, and non-activated electron transfer (ET) regime, see Fig. 1(a). Electronic overcoherence, a well-known shortcoming of the original FSSH method, is mitigated through exponential damping of the electronic amplitudes using energy-based decoherence times.[35,36] We find that FOB-SH obeys detailed balance over the entire range of diabatic electronic coupling values, but only if the the velocities are adjusted along the direction of the NACV to satisfy total energy conservation upon a surface hop. If the total kinetic energy is used, the excited state population is strongly overestimated and increases unphysically with increasing coupling due to the absence of energy-forbidden (frustrated) hops. Internal consistency is found to be good in the non-adiabatic regime, but deviations become larger in the adiabatic and non-activated regime where many of the attempted hops are energy-forbidden. Different prescriptions for velocity reversal

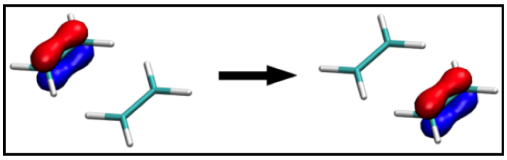

(a)

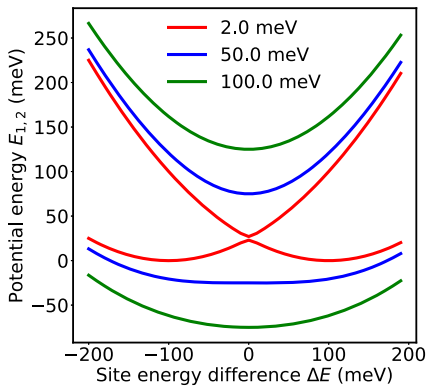

(b)

FIG. 1. Description of the model system investigated: (a) graphical representation of the two fragment orbitals for the ethylene dimer. (b) Adiabatic energy surfaces against site energy difference. Three electronic coupling values are indicated with different colours, $\lambda = 100$ meV in each case.

after frustrated hops have little influence on detailed balance and somewhat greater impact on internal consistency.

This paper is organized as follows. In Sec. II, we briefly describe the FOB-SH method followed by the derivation of the expression for the NACVs. Proofs of intermediate results are given in Appendix A. We then define the two prescriptions for determining whether a hop is energetically allowed, isotropic rescaling of the kinetic energy and velocity adjustment along the direction of the NACV, the different prescriptions for reversing of velocities following a frustrated hop, and a method for dealing with the so-called trivial crossing problem that occurs in our system for very small diabatic electronic couplings. The decoherence method is defined as well. After the description of the molecular model, force field parameters, and the details of the FOB-SH simulations in Sec. III, we present and discuss the results of our calculations in Sec. IV. Here we investigate at first the performance of the method for detection of trivial crossings by looking at the drift of the total conserved energy. Then the focus turns on the effects of the different prescriptions for velocity scaling and reversal on detailed balance and internal consistency. This is followed by a conclusion of our work in Sec. V.

II. THEORY

A. Fragment orbital-based fewest switches surface hopping (FOB-FSSH)

We have recently developed an efficient fragment orbital-based (FOB) surface hopping method specifically tailored towards the simulation of excess charge carriers in molecular materials. In the following, we summarize the most important features and formulae of our approach, which will be referred to in Secs. II B–II F. For a more detailed description of the method, we refer to our recent publication.[24] The notation we use for the different representations of the carrier wavefunction is summarized in Table I.

In FOB-SH, it is assumed that the complicated many-body electron dynamics can be effectively described by a one-particle wavefunction $\Psi(t)$ for an excess charge (electron or electron hole) moving in an effective, time-dependent potential due to the other electrons and classical nuclear motion. The remaining valence and core electrons are not explicitly treated. Their interaction with the charge carrier is included implicitly through parametrization of the electronic Hamiltonian as described further below.

In the following, we consider a molecular system composed of M "sites," e.g., molecules or molecular fragments. We assume that the charge carrier wavefunction $\Psi(t)$ can be expanded in a basis of localized, non-orthogonal fragment orbitals that mediate the charge transfer, e.g., the SOMOs of the isolated molecules $\{\varphi_m\}$,

$$\Psi(t) = \sum_{m=1}^{M} u'_m(t)\varphi_m(\mathbf{R}(t)). \tag{1}$$

Without loss of generality, we have assumed that one orbital contributes per site; more orbitals can be added in the case of (quasi-)degeneracy. In the above expression, $\mathbf{R}$ denotes the $3N$ dimensional vector of nuclear positions and the time-dependence is due to classical nuclear motion. The fragment orbital basis may be orthogonalized using Löwdin orthogonalization,

$$\phi_l = \sum_{m=1}^{M} T_{ml}\varphi_m, \tag{2}$$

where $T_{ml} = [\mathbb{S}^{-1/2}]_{ml}$ with $\mathbb{S}$ the overlap matrix with elements $S_{ml} = \langle\varphi_m|\varphi_l\rangle$. The carrier wavefunction in the orthogonal fragment orbital basis $\{\phi_l\}$ then reads

$$\Psi(t) = \sum_{l=1}^{M} u_l(t)\phi_l(\mathbf{R}(t)). \tag{3}$$

Starting from these definitions, the time-dependent Schrödinger equation takes the familiar form

$$i\hbar\dot{u}_k(t) = \sum_{l=1}^{M} u_l(t)\left(H_{kl} - i\hbar d_{kl}\right), \tag{4}$$

where H_{kl} are the elements of the electronic Hamiltonian in the $\{\phi_l\}$ basis, $H_{kl} = [\mathbb{H}]_{kl}$ and $d_{kl} = \langle\phi_k|\dot{\phi}_l\rangle$ are the non-adiabatic coupling elements (NACEs). The electronic Hamiltonian matrix is real, symmetric, and non-diagonal. In the following, we refer to the fragment orbital bases $\{\varphi_l\}$ and $\{\phi_l\}$ also as non-orthogonal and orthogonal diabatic bases, respectively, even though the NACEs d_{kl} are in general non-zero, albeit small.

A key feature of FOB-SH is that explicit electronic structure calculations of the elements H_{kl} are avoided during time propagation, which allows us to investigate large systems and long time scales. The diagonal elements $H_{kk} = \langle\phi_k|H|\phi_k\rangle$ are the energy of the excess charge localized on molecule k. We calculate this term using a classical force field where molecule k is charged and all the other $M - 1$ molecules are neutral. The off-diagonal terms $H_{kl} = \langle\phi_k|H|\phi_l\rangle$ are the electronic coupling matrix elements (also sometimes referred to as transfer integral) between the two diabatic states ϕ_k and ϕ_l. We use our recently developed analytic overlap method

TABLE I. Notation used in the three different representations of the carrier wavefunction. NACE stands for non-adiabatic coupling elements and NACV for non-adiabatic coupling vectors. Note, the diabatic representation is not strictly diabatic in the sense that the NACE vanishes; hence, it should in fact be considered as quasi-diabatic.

Representation	Basis functions	Expansion coefficients	Electronic Hamiltonian	NACE	NACV
Non-orthogonal diabatic	φ_l	u'_l	H'_{kl}	d'_{kl}	$\mathbf{d}'_{I,kl}$
Orthogonal diabatic	ϕ_l	u_l	H_{kl}	d_{kl}	$\boldsymbol{d}_{I,kl}$
Adiabatic	ψ_l	c_l	E_l	d^{ad}_{kl}	$\mathbf{d}^{\mathrm{ad}}_{I,kl}$

(AOM)[32] to calculate these terms. This method assumes a linear relationship between H_{kl} and S_{kl}, $H_{kl} = CS_{kl}$, where C is a scaling factor obtained by calibration to explicit electronic structure calculations. We found that the simple linear relationship between coupling and orbital overlap holds very well for a large number of organic pi-conjugated molecules giving mean-unsigned errors in couplings of about a factor of 2 or less. This is not too surprising as it can be shown using the working equations of, e.g., CDFT that the relation should be linear for small overlaps.[37] We refer to our previous paper[32] for a more detailed explanation of the AOM method. The NACEs d_{kl} in Eq. (4) are obtained by algebraic transformation of the NACEs in the non-orthogonal diabatic basis $\{\varphi_m\}$, $d'_{kl} \equiv [\mathbb{D}']_{kl}$,

$$d_{kl} \equiv [\mathbb{D}]_{kl} = [\mathbb{T}^\dagger \mathbb{D}' \mathbb{T}]_{kl} + [\mathbb{T}^\dagger \dot{\mathbb{S}} \mathbb{T}]_{kl}. \tag{5}$$

The elements $d'_{kl} = \langle \varphi_k | \dot{\varphi}_l \rangle$ are obtained from the finite difference of orbital overlaps using the AOM.[24]

In SH molecular dynamics, the nuclear degrees of freedom are propagated on one of the adiabatic potential energy surfaces E_i, $E_i \equiv [\mathbb{H}^{\text{ad}}]_{ii}$, where $\mathbb{H}^{\text{ad}} = \mathbb{U}^\dagger \mathbb{H} \mathbb{U}$ with $\mathbb{U}$ the unitary matrix transforming from the adiabatic electronic states $\{\psi_j\}$ to the diabatic states $\{\phi_j\}$. The nuclear forces on the adiabatic state i, $\mathbf{F}_i$, can be obtained from the gradients of the Hamiltonian matrix elements in the diabatic representation using the Hellmann-Feynman theorem

$$\mathbf{F}_{I,i} = -\nabla_I E_i = -\langle \psi_i | \nabla_I H | \psi_i \rangle = -[\mathbb{U}^\dagger (\nabla_I \mathbb{H}) \mathbb{U}]_{ii}, \tag{6}$$

where $[\nabla_I \mathbb{H}]_{kl} \equiv \nabla_I H_{kl} = \nabla_I \langle \phi_k | H | \phi_l \rangle$. The last identity in Eq. (6) has been shown explicitly in Ref. 24. In practice, the gradients of the diagonal elements, $\nabla_I H_{kk}$, are obtained from the classical force field, and the off-diagonal gradients, $\nabla_I H_{kl}$, from the finite difference of the orbital overlap using the AOM.

Finally, we give Tully's expression for the hopping probability, which needs to be evaluated every nuclear time step Δt. The probability to hop from the current (active) adiabatic state i to another state j is given by

$$g_{ji} = \frac{-2\text{Re}(a^*_{ji} d^{\text{ad}}_{ji})}{a_{ii}} \Delta t, \tag{7}$$

where $a_{ji} = c_j c_i^*$ is the electronic density matrix, and c_i are the expansion coefficients of the wavefunction Eq. (3) in the adiabatic basis, $\Psi(t) = \sum_{l=1}^{M} c_l(t) \psi_l(\mathbf{R}(t))$, where

$$\psi_l = \sum_{k=1}^{M} U_{kl} \phi_k. \tag{8}$$

Importantly, the hopping probabilities depend on the NACEs between the adiabatic states, d^{ad}_{ji}, which we obtain by transformation of the d_{kl}'s of Eq. (5),

$$d^{\text{ad}}_{ji} = [\mathbb{U}^\dagger \mathbb{D} \mathbb{U}]_{ji} + [\mathbb{U}^\dagger \dot{\mathbb{U}}]_{ji}. \tag{9}$$

This completes our description of the FOB-SH method implemented in previous work.[24] In summary, in our approach, the time dependent electronic wavefunction is expanded and the electronic Hamiltonian and NACEs are constructed in the (quasi)-diabatic basis of fragment orbitals. The time-dependent electronic Schrödinger equation is then solved in the same diabatic basis. At each nuclear time step, the electronic wavefunction and NACEs as well as the nuclear forces are transformed from the diabatic to the adiabatic representation for calculation of the hopping probabilities and for propagation of the nuclei, respectively. Solving the electronic Schrödinger equation in the diabatic rather than adiabatic representations has the advantage of greater numerical stability.[38–40] At avoided crossings, the adiabatic NACE can be strongly peaked which can be easily missed unless the nuclear time step is chosen very small. By contrast, the NACEs between the (quasi-)diabatic states remain small at avoided crossings (or vanish for truly diabatic states). In this representation, the transition between electronic states is due to the diabatic electronic couplings, which usually vary smoothly along the trajectory. This practical advantage has led to the development of "local diabatization" in quantum chemical applications of surface hopping.[38,39] At each nuclear time step, the adiabatic states obtained from quantum chemistry are transformed to a diabatic basis in which the electronic wavefunction is propagated, followed by transformation back to the adiabatic basis. The first transformation is not needed in our approach as we directly construct the Hamiltonian in a diabatic basis.

B. NACVs between adiabatic states

The surface hopping algorithm defined by Eqs. (4), (6), and (7) does not require the calculations of the non-adiabatic coupling vectors (NACVs), merely the scalar non-adiabatic coupling elements Eqs. (5) and (9). However, Tully[9] noted that a hop between two surfaces should occur only if there is enough kinetic energy in the direction *parallel* to the NACVs between the two adiabatic states in question. Moreover, it was suggested that the velocity component parallel to the NACV should be inverted if a hop cannot occur due to insufficient kinetic energy.[41] These prescriptions make it necessary to compute the NACVs between the active adiabatic state and all other adiabatic states every nuclear time step. In the following, we outline how this can be done within the FOB-SH framework. A detailed derivation of every step is given in Appendix A.

We start with the following, well-known identity for the NACV on atom I between the adiabatic states i and j,

$$\mathbf{d}^{\text{ad}}_{I,ij} = \frac{1}{E_j - E_i} \left\langle \psi_i | \nabla_I H | \psi_j \right\rangle. \tag{10}$$

The right hand side (RHS) of Eq. (10) cannot be calculated directly in our approach as we know H only in terms of matrix elements in the diabatic basis $\{\phi\}$ (note, here H is not an *ab initio* Hamiltonian). We will show in the following that the RHS of Eq. (10) can be written solely in terms of gradients in the diabatic basis sets $\{\phi\}$ and $\{\varphi\}$, which are readily available in our scheme. We first transform the RHS of Eq. (10) to the $\{\phi\}$ basis. Insertion of the unitary transformation Eq. (8) in Eq. (10) followed by some algebraic manipulations [see Eqs. (24)–(26) in Ref. 24 or Appendix A], we obtain

$$\mathbf{d}^{\text{ad}}_{I,ij} = \frac{1}{E_j - E_i} [\mathbb{U}^\dagger \mathbb{G}_I \mathbb{U}]_{ij}, \tag{11}$$

$$\mathbb{G}_I = \nabla_I \mathbb{H} + [\mathbb{D}_I, \mathbb{H}], \tag{12}$$

where $\nabla_I \mathbb{H}$ was defined in Eq. (6), $[\mathbb{D}_I]_{kl}$ is the NACV in the $\{\phi\}$ basis,

$$[\mathbb{D}_I]_{kl} = \langle \phi_k | \nabla_I \phi_l \rangle, \tag{13}$$

and $[\ldots,\ldots]$ denotes the commutator. The term involving the commutator can be simplified (see Appendix A), which results in the final expression for the NACV between the adiabats in terms of derivatives in the $\{\phi\}$ basis

$$\mathbf{d}^{\mathrm{ad}}_{I,ij} = \mathbf{a}^{\mathrm{ad}}_{I,ij} + \mathbf{b}^{\mathrm{ad}}_{I,ij}, \tag{14}$$

$$\mathbf{a}^{\mathrm{ad}}_{I,ij} = \frac{1}{E_j - E_i}[\mathbb{U}^\dagger \nabla_I \mathbb{H} \mathbb{U}]_{ij}, \tag{15}$$

$$\mathbf{b}^{\mathrm{ad}}_{I,ij} = [\mathbb{U}^\dagger \mathbb{D}_I \mathbb{U}]_{ij}. \tag{16}$$

The first term, Eq. (15), resembles the nuclear force expression Eq. (6), except that it couples two different adiabatic electronic states and contains a division by the energy difference. The matrices $\nabla_I \mathbb{H}$ and $\mathbb{U}$ appeared already in the nuclear forces calculation [Eq. (6)]; hence, they are readily available. The second term, Eq. (16), cannot be calculated directly and requires transformation of $\mathbb{D}_I$ from the orthogonal $\{\phi\}$ to the non-orthogonal $\{\varphi\}$ basis. Insertion of Eq. (2) in Eq. (13) and application of the chain rule give

$$\mathbb{D}_I = \mathbb{T}\mathbb{D}'_I\mathbb{T} + \mathbb{T}^{-1}\nabla_I\mathbb{T}, \tag{17}$$

where

$$[\mathbb{D}'_I]_{kl} = \langle \varphi_k | \nabla_I \varphi_l \rangle. \tag{18}$$

Insertion of Eq. (17) in Eq. (16) gives

$$\mathbf{b}^{\mathrm{ad}}_{I,ij} = [\mathbb{U}^\dagger \mathbb{T}\mathbb{D}'_I\mathbb{T}\mathbb{U}]_{ij} + [\mathbb{U}^\dagger \mathbb{T}^{-1}\nabla_I\mathbb{T}\mathbb{U}]_{ij}. \tag{19}$$

The NACVs in the $\{\varphi\}$ basis, Eq. (18), can be obtained from the AOM [Eqs. (43) and (44) in Ref. 24]. The only remaining expression in Eq. (19) that is not readily available is the nuclear gradient of the Löwdin transformation matrix, $\nabla_I\mathbb{T}$. However, as shown in Appendix A. $\nabla_I\mathbb{T}$ can be written exactly in terms of the gradient of the overlap matrix, $\nabla_I\mathbb{S}$. The final expression for $\mathbf{b}^{\mathrm{ad}}_{I,ij}$ then becomes

$$\mathbf{b}^{\mathrm{ad}}_{I,ij} = [\mathbb{U}^\dagger \mathbb{T}\mathbb{D}'_I\mathbb{T}\mathbb{U}]_{ij} + [\mathbb{U}^\dagger \mathbb{L}\mathbb{W}'_I\mathbb{L}^\dagger\mathbb{U}]_{ij}, \tag{20}$$

where

$$(\mathbb{W}'_I)_{kl} = -\frac{[\mathbb{T}^{\mathrm{diag}}]_{kk}([\mathbb{T}^{\mathrm{diag}}]_{ll})^2}{[\mathbb{T}^{\mathrm{diag}}]_{kk} + [\mathbb{T}^{\mathrm{diag}}]_{ll}}[\mathbb{L}^\dagger\nabla_I\mathbb{S}\mathbb{L}]_{kl} \tag{21}$$

and $\mathbb{L}$ the matrix that diagonalizes the Löwdin transformation matrix $\mathbb{T}$, $\mathbb{T}^{\mathrm{diag}} = \mathbb{L}^\dagger\mathbb{T}\mathbb{L}$. Equation (14) together with Eqs. (15) and (20) is the main result of this paper. These expressions allow us to calculate the adiabatic NACVs in a way that is consistent with the calculation of nuclear forces in Eq. (6), using the gradients in the diabatic representation.

We note that the calculation of the second term on the RHS of Eq. (20) involves a series of matrix-matrix multiplications, which is computationally expensive. Fortunately, as we will show in Sec. IV, the term $\mathbf{b}^{\mathrm{ad}}_{I,ij}$ is typically very small and can be neglected. This term pertains to the $\mathbb{D}_I$ matrix that quantifies the response of the diabatic electronic states to a small displacement of the atoms. The localized nature of these states makes this response small and $\mathbf{b}^{\mathrm{ad}}_{I,ij}$ negligible.

C. Energy conservation after a successful hop

Electronic transitions occur on the sub-femtosecond time scale and are much faster than typical nuclear frequencies. Hence, it can be argued that when a hop between two electronic states occurs, the potential energy difference cannot be provided sufficiently fast through coupling with an external heat bath with typical nuclear relaxation times. Instead, the potential energy difference should be compensated by a change in the nuclear kinetic energy of the system. This leads to the following condition for the conservation of total energy:

$$E_{\mathrm{tot}}(\mathbf{R}) = T_a(\mathbf{R}) + E_a(\mathbf{R}) = T_n(\mathbf{R}) + E_n(\mathbf{R}), \tag{22}$$

where E_a and E_n are the adiabatic potential energies before and after a hop, respectively (subscript "a" for "active," "n" for "new") and T_a and T_n are the nuclear kinetic energies before and after a hop, $T_a = \sum_I (M_I/2)\dot{\mathbf{R}}^2_{I,a}$, $T_n = \sum_I (M_I/2)\dot{\mathbf{R}}^2_{I,n}$, M_I is the mass of atom I. If the potential energy gap between the attempted new state n and the former active state a is larger than the nuclear kinetic energy T_a, the hop is termed "energetically forbidden" and is rejected. Tully *et al.* underlined the role of those rejected hops to reach detailed balance between the different electronic states.[34,42]

In the literature, several prescriptions exist to determine if a hop is allowed energetically, mainly of two kinds: isotropic rescaling of the full velocity vector for each atom and rescaling of the velocity component parallel to a given vector for each atom. According to the theoretical work of Pechukas,[43] Herman,[44,45] and Coker and Xiao,[46] the nuclei feel forces proportional to the NACV during an infinitely fast hop between two surfaces. Tully's original work[9] adopts this theory and rescales the velocity component parallel to the NACV for each atom. Hack *et al.*[47] have benchmarked different vectors for the velocity rescaling and obtained best results when the velocity component along the NACV is scaled. In the following, we will consider only the two most common prescriptions: (i) isotropic rescaling and (ii) NACV-oriented rescaling.

According to the isotropic rescaling prescription, all the post-hop velocities would be scaled with the same factor κ, $\dot{\mathbf{R}}_{I,n} = \kappa\dot{\mathbf{R}}_{I,a}$. Requiring conservation of total energy, Eq. (22), gives

$$\kappa = \sqrt{1 - \frac{\Delta V}{T_a}}, \tag{23}$$

where $\Delta V = E_n - E_a$. If $\Delta V > T_a$, the hop is rejected, and if the new state is lower in energy, $\Delta V < 0$, the hop is always successful. The practical advantage of isotropic rescaling is that NACV vectors are not needed for velocity rescaling. However, a serious deficiency of isotropic rescaling is the size extensivity of the energy criterion. For instance, the more solvent molecules are included in the FSSH simulation, the more kinetic energy is available and the fewer hops are energy forbidden. This is clearly unphysical as the water molecules far away from the reactive region should not affect the nonadiabatic dynamics (apart from changing slightly the potential energy).

The problem with size extensivity is avoided if only the velocity component in the direction of the NACV ($\mathbf{d}^{\mathrm{ad}}_{I,an}$) is

adjusted

$$\dot{\mathbf{R}}_{I,n} = \dot{\mathbf{R}}_{I,a} + \gamma \frac{\mathbf{d}^{\mathrm{ad}}_{I,an}}{M_I}, \tag{24}$$

where $\mathbf{d}^{\mathrm{ad}}_{I,an}$ is defined in Eq. (10) and calculated within the FOB-SH framework according to Eq. (14). Inserting Eq. (24) into Eq. (22) leads to a quadratic equation for the scaling factor γ,[18]

$$A\gamma^2 + B\gamma + \Delta V = 0, \tag{25}$$

$$A = \sum_I \frac{|\mathbf{d}^{\mathrm{ad}}_{I,an}|^2}{2M_I}, \tag{26}$$

$$B = \sum_I \mathbf{d}^{\mathrm{ad}}_{I,an} \cdot \dot{\mathbf{R}}_I. \tag{27}$$

If $(B^2 - 4A\Delta V) \geq 0$ Eq. (25) has real solutions: $\gamma = (-B \pm \sqrt{B^2 - 4A\Delta V})/2A$. Following Fabiano *et al.*,[18] we take the solution with the smallest absolute value. If $(B^2 - 4A\Delta V) < 0$, no real solution exists which means there is not enough kinetic energy along the NACV to satisfy energy conservation, in which case the hop is rejected.

D. Velocity reversal after a rejected hop

A rejected hop may be interpreted as to a nuclear trajectory trying to reach the upper state along the direction of the NACV and bouncing back due to the lack of kinetic energy along that direction. Tully suggested to always reverse the velocity component along the NACV direction if an attempted hop is rejected[41]

$$\dot{\mathbf{R}}_{I,n} = \dot{\mathbf{R}}_{I,a} - 2\frac{\dot{\mathbf{R}}_{I,a} \cdot \mathbf{d}^{\mathrm{ad}}_{I,an}}{|\mathbf{d}^{\mathrm{ad}}_{I,an}|^2}\mathbf{d}^{A}_{I,an}. \tag{28}$$

Jasper and Truhlar[48] decided to use a more restrictive approach to velocity reversal, apparently to improve the agreement with an exact quantum calculation.[49] They suggested to reverse the velocities after a frustrated hop according to Eq. (28) only if the velocities and the nuclear forces in the new state have opposite sign, i.e., if the following condition is fulfilled:

$$\left(\sum_I \mathbf{d}^{\mathrm{ad}}_{I,an} \cdot \dot{\mathbf{R}}_{I,a}\right)\left(\sum_I \mathbf{d}^{\mathrm{ad}}_{I,an} \cdot (-\nabla_I E_n)\right) < 0\ . \tag{29}$$

Finally, Jain and Subotnik[50] added a second condition,

$$\left(\sum_I \mathbf{d}^{\mathrm{ad}}_{I,an} \cdot (-\nabla_I E_a)\right)\left(\sum_I \mathbf{d}^{\mathrm{ad}}_{I,an} \cdot (-\nabla_I E_n)\right) < 0. \tag{30}$$

We will consider in Sec. IV D the effect of the suggested reversing prescriptions on detailed balance and internal consistency.

E. Decoherence correction

A well-documented deficiency of FSSH is electronic overcoherence, which is a consequence of the classical treatment of nuclear motion.[51–53] In a fully quantum mechanical treatment, after passing an avoided crossing, the nuclear wave packet settles on one of the adiabatic electronic states and the off-diagonal elements of the electronic density matrix (in the adiabatic representation), a_{ij}, decay to zero. In contrast, in FSSH, a_{ij} remains finite. Several correction schemes have been suggested to address the decoherence problem in FSSH ranging from instant collapse of the electronic wave function to the active state[52,54,55] to exponential damping of the inactive electronic states (e.g., coherent switching with decay of mixing approach[53] and energy-based decoherence correction[35,53,56]) and augmented FSSH (a-FSSH).[57,58]

In this work, we apply the energy-based decoherence correction suggested by Truhlar *et al.*,[53,56] which is frequently used in the literature.[59,60] At each nuclear time step Δt, the electronic coefficients in the diabatic basis, u_k, obtained by solving Eq. (4), are transformed to the adiabatic basis, c_i, which are used to compute the hopping probabilities Eq. (7) for determination of the active state a. Then all non-active states $i \neq a$ are exponentially damped,

$$c_i \rightarrow c_i \exp(-\Delta t/\tau_{ia}). \tag{31}$$

The coefficient for state a, c_a, is scaled appropriately to ensure norm conservation, see, e.g., Ref. 35 for an explicit expression. Thereafter, the wavefunction is transformed back to the diabatic basis and propagated further in time by solving Eq. (4). The decoherence time τ_{ia} is inversely proportional to the energy gap and reads

$$\tau_{ia} = \frac{\hbar}{|E_i - E_a|}\left(C + \frac{E_0}{T_a}\right), \tag{32}$$

where T_a is the nuclear kinetic energy and C and E_0 are suitably chosen parameters.

F. Detection of trivial crossings

A trivial or unavoided crossing refers to the situation in which the energy gap between two adiabatic surfaces is very small or even disappears, e.g., at a conical intersection or seam. The NACV, being inversely proportional to the energy gap between the two surfaces [see Eq. (10)], becomes very large and the NACE goes through a sharp maximum at this point (assuming the velocities are not exactly orthogonal to the NACV). Consequently, the hopping probability Eq. (7) reaches unity, meaning a hop should occur with certainty. However, in practice, the sharp peak in NACE could go unnoticed due to the finite nuclear time step used to integrate the nuclear equations of motion. In this case, the trivial crossing is missed and the system is most likely to remain on the same surface. This causes several artifacts: it leads to an unwanted bias in the population of excited electronic states, to a discontinuity in the nuclear forces, and to spurious long-range charge transfer events.

A trivial but computationally prohibitive solution to the trivial crossing problem is to use small enough integration time steps. More useful approaches to solve this problem have been suggested in the literature, e.g., detection of unphysical discontinuities of the involved PESs,[61] detection of discontinuities in the overlap of the active adiabatic states at consecutive time steps,[60,62] flexible surface hopping,[63] norm-preserving interpolation of the adiabatic electronic wavefunctions within each time step for more accurate calculation of NACE,[64] and self-consistent surface hopping.[65] We have implemented the latter method that was recently suggested by Wang and Prezhdo.

It is based on the exact sum rule for Tully surface hopping probabilities,

$$\sum_{k\neq a} g_{ka} = -\frac{\mathrm{d}|c_a|^2/\mathrm{d}t}{|c_a|^2}\mathrm{d}t, \tag{33}$$

which can be easily derived by summing the hopping probabilities Eq. (7) from the active state a to all other states k and substituting the time-dependent Schrödinger equation in the density matrix form, $\dot{a}_{aa} = -2Re\left(\sum_{k\neq a} d^{\mathrm{ad}}_{ak} a_{ka}\right)$, where $a_{ka} = c_k c_a^*$. The sum rule states that the change in the probability of the active state [RHS of Eq. (33)] should be equal to the quantum flux of leaving the active state [LHS of Eq. (33)]. The crucial point is that the sum rule is violated as soon as a hopping probability is not calculated accurately as, for instance, in the case of a trivial crossing. To impose Eq. (33) at each time step, the probability to hop to the state closest in energy to the active state, denoted state j, is modified accordingly,

$$g_{ja} = -\frac{\mathrm{d}|c_a|^2/\mathrm{d}t}{|c_a|^2}\mathrm{d}t - \sum_{k\neq a,j} g_{ka}. \tag{34}$$

This way, an accurate calculation of the NACE between states a and j is no longer required. While effective, inexpensive, and easy to implement, the method assumes that the hopping probabilities from state a to all states other than j are accurate. Hence, the method will no longer work if more than two states form an avoided crossing, but this is expected to occur only rarely. Equation (34) is implemented using finite differences and is applied routinely at each MD time step. We will discuss the performance of this correction scheme in more detail in Sec. IV B.

III. SIMULATION DETAILS

A. Model system

We have investigated detailed balance, internal consistency, and energy conservation for electron hole transfer in a dimer of ethylene-like molecules (ELMs), embedded in a bath of 124 neon atoms. The center of mass of the two ELMs is restrained with a weak restraining potential centered at 3.6 Å (force constant = 11 kcal mol^{-1} Å^{-2}). A similar model system without Ne atoms was chosen in our previous studies.[24,66] We refer to the molecules as "ethylene-like" because only their nuclear geometries correspond to real ethylene molecules. The reorganization energy λ and the constant C determining the magnitude of diabatic electronic couplings, H_{kl}, are chosen freely to simulate hole transfer in different parameter regimes. The Ne atoms take the role of a heat bath facilitating energy exchange with the ELMs while running the FOB-SH simulation in the NVE ensemble. This way we avoid the introduction of artificial bias forces due to the thermostat. We used a cubic box of length 60 Å which corresponds to a density of 6.3×10^{-4} atoms Å^{-3}. A snapshot of the dimer can be found in Fig. 1(a).

B. Force field parameters

We assume that the electron hole transfer is mediated by the HOMOs of the ethylene molecules, φ_1 and φ_2. They are used as basis functions for the expansion of the charge carrier wavefunction according to Eq. (1). The diagonal elements of the corresponding 2×2 electronic Hamiltonian H_{kk}, $k = 1, 2$ are estimated using two classical potential energy functions (force fields). In force field 1 (2), ELM 1 (2) is neutral and ELM 2 (1) is positively charged, giving the site energies H_{11} (H_{22}) and the corresponding forces $\nabla_I H_{11}$ ($\nabla_I H_{22}$). Intra-molecular interactions for the neutral ELM are taken from the Generalized Amber Force Field (GAFF).[67] The same intramolecular parameters are taken for the charged ELM except for the carbon-carbon bond length which was chosen to obtain a reorganization energy λ for electron hole transfer of λ = 0.1 eV (at infinite donor-acceptor distance). This requirement gave a carbon-carbon bond length of 1.369 Å for the charged ELM, compared to 1.324 Å for the neutral molecule. The intermolecular interaction between the ELMs and between ELM and Ne atoms is modeled by Lennard-Jones terms with parameters taken from the GAFF database for neutral and charged ELMs and from Ref. 68 for Ne and applying the Lorentz-Berthelot mixing rules. Electrostatic interactions in the form of fixed point charges do not significantly alter the energetics of this system because only one ELM carries a net charge and the other ELM and Ne are charge neutral. Hence, for convenience, electrostatic interactions were switched off. The off-diagonal element of the Hamiltonian, H_{12}, is calculated using the AOM.[32] Briefly, the HOMOs of the ELMs, φ_1 and φ_2, are calculated with the PBE functional and expanded in a minimum Slater basis of p orbitals and updated along the trajectory as described in detail in Ref. 24. H_{12} is obtained via the simple linear relationship $H_{12} = CS_{12}$, with $S_{12} = \langle\varphi_1|\varphi_2\rangle$ calculated analytically. The coupling derivatives $d'_{I,12} = \langle\varphi_1|\nabla_I\varphi_2\rangle$ are obtained using finite differences of the AOM overlap and are used for the calculation of $\nabla_I S_{12}$, $\nabla_I H_{12}$, $\boldsymbol{d}_{I,12}$, and $\mathbf{d}^{\mathrm{ad}}_{I,12}$. The NACEs d^{ad}_{12} are calculated similarly using finite differences. A detailed description of these calculations is given in Ref. 24. FOBSH simulations were carried out for different values of the scaling factor C, appropriately chosen to obtain average electronic coupling matrix elements, $\langle H^2_{\mathrm{ab}}\rangle^{1/2}$, between λ and $\lambda/1000$, while keeping the reorganization energy λ constant at 0.1 eV. The scaling values used are C = 0.03, 0.02, 0.01, 0.008, 0.003, 5×10^{-4}, 5×10^{-5} Ha. This allows us to investigate the different regimes of electron transfer, from non-adiabatic to adiabatic to non-activated.

C. Preparation of initial structures

To investigate the properties of FOB-SH in thermal equilibrium, we prepared initial structures drawn from a thermally equilibrated distribution of positions, velocities, and adiabatic states. We built the initial configuration from two ELMs in their energy-minimized geometry, surrounded by Neon atoms positioned in a regular grid. The system is equilibrated to 300 K for 1 ns in the *NVT* ensemble using a Nosé-Hoover thermostat.[69,70] Then, 100 ps Born-Oppenheimer molecular dynamics for both the ground (E_0) and excited (E_1) adiabatic electronic states of the charged system is carried out using forces calculated according to Eq. (6). This is done for each of the seven scaling values C that determines the strength of electronic coupling (see Sec. III B). We remove the first 40 ps where the system

equilibrates and use the last 60 ps of the ground state trajectories to calculate the free energy between ground and excited state, $\Delta A_{10}(C) = -k_B T \ln \langle \exp[-(E_1 - E_0)/k_B T] \rangle_{E_0}$, for each scaling value C. The corresponding 'exact' excited state population is determined as $P_1(C) = 1/(1 + \exp(\Delta A_{10}(C)/k_B T))$, which will serve as reference values for the excited state population obtained from FOB-SH. We extracted $1000(1 - P_1(C))$ configurations (nuclear coordinates and velocities) from the last 60 ps of the ground state run and $1000P_1(C)$ configurations from the last 60 ps of the excited state run as starting configurations for the FOB-SH runs. This ensures that the FOB-SH simulations are initiated at $t = 0$ from an ensemble with exact excited state population. The electronic wavefunction is initialized in the corresponding adiabatic state $\Psi(0) = \psi_0$ or ψ_1 to ensure perfect internal consistency at $t = 0$.

D. FOB-SH simulations

The methodological improvements to FOB-SH described in Secs. II B–II F have been implemented in the CP2K simulation package.[71] We generated 1000 independent trajectories for each set of parameters investigated starting from initial structures that were prepared as described in Sec. III C. Unless stated otherwise, simulations have been carried out with the following default settings. The nuclear dynamics is propagated with the velocity-Verlet algorithm with forces calculated according to Eq. (6) and with an MD time step $\Delta t = 0.5$ fs. The simulations are run in the NVE ensemble with the temperature remaining approximately constant at around 300 K due to interaction with the bath of Ne atoms. Surface-hopping probabilities are calculated according to Eq. (7) every MD time step. The probability for a hop to the state closest in energy to the current state is replaced by the expression, Eq. (34) (in accord with the SC-FSSH method). Velocity adjustment according to Eq. (24) was considered to determine whether a hop was energy-allowed. Whenever a hop was energy-forbidden, the velocities were reversed in accord with Eq. (28). The wavefunction of the excess charge carrier Eq. (3) was propagated by integrating Eq. (4) using the Runge-Kutta algorithm of 4th order and an electronic time step $\delta t = \Delta t/5 = 0.1$ fs. We investigated smaller electronic time steps ($\Delta t/10$ and $\Delta t/50$), but we did not observe any noticeable change for the energy conservation or for the excited state population. An interpolation scheme is used to calculate the Hamiltonian matrix elements at each electronic time step, as explained in our previous work.[24] A decoherence correction to the electronic propagation is applied according to Eq. (31) with a decoherence time defined in Eq. (32) setting $C = 1$ and $E_0 = 0.1$ H. We found that excited state populations are well converged within 10 ps of simulation time and an ensemble of 200 trajectories. Error bars were determined by block averaging of the 1000 trajectories with a block size of 200 independent trajectories.

IV. RESULTS AND DISCUSSION

A. NACV: Importance of $\mathbf{b}^{\mathrm{ad}}_{I,ij}$ [Eq. (14)]

To investigate the importance of the lengthy term $\mathbf{b}^{\mathrm{ad}}_{I,ij}$ in the expression for the adiabatic NACVs [Eq. (14)], we generated three FSSH runs of 100 ps length with average couplings of $\langle |H_{12}|^2 \rangle^{1/2} = 0.34$, 1.7, and 10.0 meV. Approximately 8000 attempted hops are recorded in total. For each attempted hop, we calculate the error between the total NACV $\mathbf{d}^{\mathrm{ad}}_{I,ij}$, Eq. (14), and the NACV with the term $\mathbf{b}^{\mathrm{ad}}_{I,ij}$ neglected, hereafter referred to as "fast NACV" calculation. The relative error of the fast NACV calculation is defined as $\epsilon = |\mathbf{b}^{\mathrm{ad}}_{I,ij}|/|\mathbf{d}^{\mathrm{ad}}_{I,ij}|$. We find that the median of the error is negligibly small, about 3×10^{-4} for all three coupling values. We also checked the influence of the fast NACV calculation on the kinetic energy criterion Eq. (25) determining whether a hop is energy-allowed. Only 0.05% of decisions differ using the fast NACV calculation. Finally, Fig. 3 shows the excited state population for different electronic coupling values using velocity adjustment along the direction of the NACV. The two curves obtained using total NACV and fast NAVC are indistinguishable from one another. Hence, we conclude that the term $\mathbf{b}^{\mathrm{ad}}_{I,ij}$ in Eq. (14) can be safely neglected.

We have used the same simulation data to obtain the average NACE in the three different representations of electronic states, non-orthogonal diabatic, orthogonal diabatic, and adiabatic, $\sqrt{\langle d^2 \rangle}$, where d is d'_{ij}, d_{ij}, or d^{ad}_{ij}. We obtained values of 0.3 meV/$\hbar$ for d'_{ij} and d_{ij} and 132 meV/$\hbar$ for d^{ad}_{ij}. The small values obtained for d'_{ij} imply that the SOMOs are a relatively good approximation to the true diabatic states ($d = 0$) and that orthogonalization has only a small or negligible effect. As expected, the average NACE between the adiabats is much larger as it couples the electronic states in this representation. It is dominated by the time derivative of the unitary transformation matrix, second term in Eq. (9), while the first term involving the transformation of d_{ij} is negligibly small.

B. Trivial crossings and choice of MD time step

Before assessing the effect of different velocity rescaling/reversing prescriptions on detailed balance and internal consistency, we determine the optimal MD time step to use in our simulations, as well as the benefits of the SC-FSSH method in addressing the trivial crossing problem (see Sec. II F). To this end, we have carried out FOB-SH simulations with and without the self-consistency (SC) correction for hopping probabilities Eq. (34) using MD time steps of 0.05, 0.1, and 0.5 fs. See Sec. III D for further simulation details. For each run, we have estimated the total energy drift via the absolute value of the slope of the total energy divided by the total number of electronically active atoms in our simulation (2 ELMs, i.e., 12 atoms).

Figure 2(a) shows the energy drift averaged over 1000 FOB-SH NVE runs as a function of electronic coupling. We first discuss the results obtained without the SC correction (red lines). We find that at very large coupling values, the total energy drift is small for all three time steps ($<10^{-6}$ Ha/ps/QM atom) with the drift slightly increasing for increasing Δt. In this regime, only a few hopping events occur and the dynamics is essentially adiabatic and governed by the Born-Oppenheimer ground state. The quality of energy conservation is not at the same level as for MD with standard force fields (10^{-12} Ha/ps/atoms for this code), most likely because of the finite difference approach we used to calculate the gradient of the

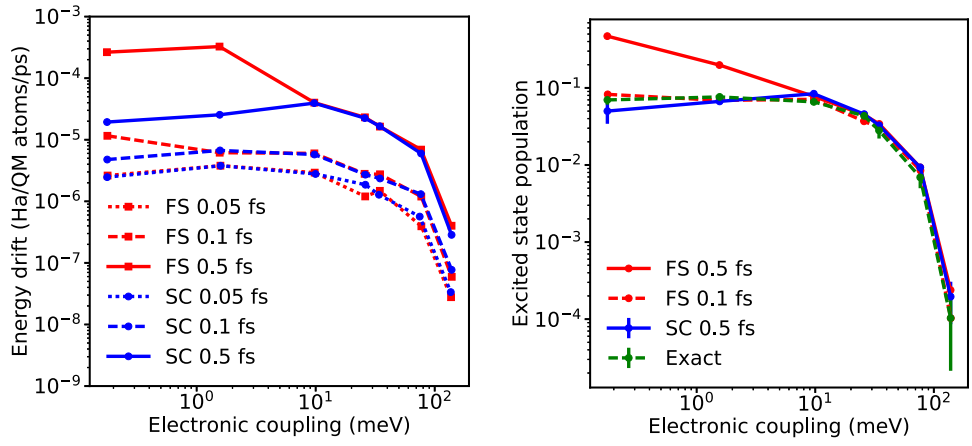

FIG. 2. Influence of the nuclear time step and of the surface hopping method on (a) energy drift and (b) excited state population for different diabatic electronic couplings. FS indicates results obtained with the FOB-SH method and SC results obtained with the self consistent FOB-SH method (see Sec. II F), while the number in femtosecond is the nuclear time step. Results are obtained for electron hole transfer in a dimer of ethylene-like molecules solvated in a bath of Ne atoms [see Fig. 1(a)]. Error bars are shown for our default option (SC 0.5 fs) and represent standard deviations over five independent blocks of 200 trajectories. Error bars for the exact population indicate standard deviation over three blocks of 20 ps.

off-diagonal elements of the Hamiltonian. When electronic coupling is decreased from 100 meV to 0.1 meV, the energy drift increases by about two orders of magnitudes, independently on the time step used. This can be explained by two effects: (i) the number of successful hops increases as the energy gap between the adiabatic surface decreases leading to discontinuity in the forces and (ii) the potential energy surfaces form a cusp in the transition state region (diabatic energy gap $\Delta E = 0$), and trivial crossings are missed if the time steps are too large. This leads to discontinuities in the forces.

The energy drifts obtained with the SC correction to trivial crossings are shown in blue lines. For the smallest time step chosen, the SC corrected results coincide with the uncorrected results down to the smallest couplings. This shows that uncorrected FOB-SH with a small time step of 0.05 fs can capture the trivial crossings and the SC correction does not improve energy conservation further [i.e., the drift is due to explanation (i) above]. Yet, SC becomes very effective for larger time steps. At $\Delta t = 0.5$ fs, the SC correction reduces the drift by 1 order of magnitude for small couplings as trivial crossings are correctly detected [mitigating point (ii) above].

The SC correction also improves detailed balance. In Fig. 2(b), we show the excited state population averaged over time and over 1000 trajectories. FOB-SH without SC correction reproduces correctly the exact result if a small time step of 0.1 fs is used. However, with a larger time step, $\Delta t = 0.5$ fs, the exact population is overestimated by a factor of 2 for the lowest coupling value. This is because more trivial crossings are missed from the excited to the ground state than the other way round as the nuclear trajectory oscillates around the crossing region in the excited state. Adding the SC correction removes this artefact and reproduces correctly the excited state population. Hence, the SC correction allows us to use about 5 times larger MD time steps without deteriorating detailed balance and energy conservation.

C. Kinetic energy criterion for allowed hops

We now compare the two different criteria used in the literature to determine whether a hop is energetically allowed: isotropic rescaling of the full velocity vector and rescaling of the component parallel to the NACV to conserve total energy. FOB-SH simulations were carried out for these two prescriptions, with all other simulation details given in Sec. III D. Figure 3 shows the excited state populations obtained as a function of electronic coupling, together with the exact populations obtained from the free energy calculation described in Sec. III C. The latter decreases by four orders of magnitudes when the electronic coupling (and thus the gap between the surfaces) is increased from 0.2 to 100 meV. We find that

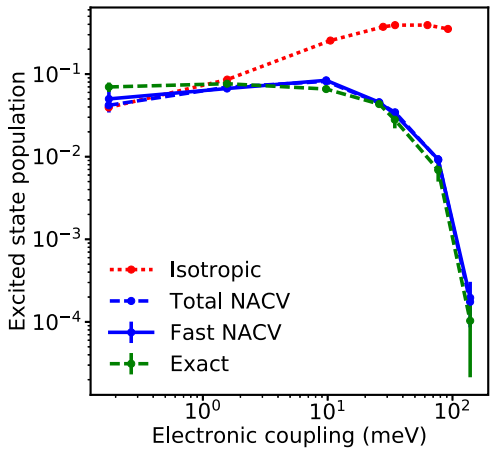

FIG. 3. Influence of the rescaling prescription used to ensure energy conservation on excited state population for different diabatic electronic couplings. "Isotropic" results use the isotropic rescaling with the factor given in Eq. (23). "Fast NACV" and "total NACV" refer to rescaling along the direction of the NACV, Eq. (24). In the former case, NACVs are calculated according to Eq. (14) with $b^{ad}_{I,ij}$ set to zero, while in the latter case all terms in Eq. (14) are calculated. Error bars are shown for our default option (fast NACV) and represent standard deviations over five independent blocks of 200 trajectories. Error bars for the exact population indicate standard deviation over three blocks of 20 ps.

the energy criterion based on the NACV reproduces the exact populations very well in all coupling regimes, with and without decoherence correction. The deviation is typically within the error bars of our simulations.

Turning to isotropic rescaling, we find that the excited state populations are well reproduced only for a small coupling value of up to 2 meV. For larger values, the populations increase rather than decrease, strongly overestimating the exact results. This unphysical behaviour can be rationalized as follows. In the isotropic rescaling method, a hop is successful if the kinetic energy of the quantum subsystem is larger than the adiabatic energy gap between the states. Estimating the average kinetic energy for the 2 ELMs as $T_a \approx 12 \times 3 \times k_B T/2 = 450$ meV, we find them to be larger than the average adiabatic energy gaps at the crossing regions, $2H_{12} = 0.4 - 200$ meV, for the range of coupling values investigated. Hence, virtually all attempted hops will be energy-allowed, even for the systems with large energy gaps. By contrast, when velocities are adjusted along the NACV direction, a hop is successful only if Eq. (25) is fulfilled. This equation can be written as $B^2/(4A) > \Delta V$, where ΔV is the adiabatic energy gap between the states. We have derived the thermal average of the ratio $B^2/(4A)$ (see Appendix B): $\langle B^2/(4A)\rangle = k_B T/2 \approx 13$ meV. Hence, unsuccessful (or frustrated) hops should become important when the gap is larger than 13 meV, i.e., when the coupling value is larger than 6 meV. This is precisely where the isotropic scaling method starts to deviate from the exact results, see Fig. 3. This analysis emphasizes the importance of energy-forbidden (frustrated) hops for achieving detailed balance in FOB-SH, especially when diabatic electronic coupling values are large.

The rescaling of the velocities along the component parallel to the NACV is a key feature of the original Tully method[9] and relies on different theoretical derivations. This feature was shown essential to compare the FSSH results with quantum calculation.[47] The present work complements the previous analysis and demonstrates that this feature is also required to achieve detailed balance.

D. Velocity reversal after a rejected hop

Finally, we consider different treatments of velocities after an attempted hop is deemed energy-forbidden, i.e., rejected. Tully suggested to always reverse the velocities along the NACV direction according to Eq. (28). But some authors suggested to reverse the velocities only if some criteria are fulfilled as detailed in Sec. II D. To investigate the effect of velocity reversal, we define four different treatments: (i) never reverse the velocities (N), (ii) always reverse the velocities (A), (iii) reverse them according to the criterion suggested by Truhlar (T), Eq. (29), and (iv) reverse them according to the criteria suggested by Subotnik (S), Eqs. (29) and (30). FOB-SH simulations were carried out for these different treatments. Simulation details are given in Sec. III D.

While the four prescriptions for velocity reversal give virtually identical results for energy drift and detailed balance, we find that they give somewhat different results for internal consistency. To quantify the error, we calculated the time-averaged root mean square error (RMSE) between the surface population and the quantum amplitude of the excited state, $P_1(t)$ and $\langle|\psi_1(t)|^2\rangle_{\text{trj}}$, respectively,

$$\text{RMSE} = \left(\frac{1}{T}\int_0^T \mathrm{d}t \left(P_1(t) - \langle|\psi_1(t)|^2\rangle_{\text{trj}}\right)^2\right)^{1/2}, \qquad (35)$$

where $\langle\ldots\rangle_{\text{trj}}$ refers to an average over trajectories. Figure 4(a) shows the RMSE obtained for the usual range of coupling values and Fig. 4(b) shows the RMSE normalised with respect to the exact excited state population, RMSE/P_1^{ex}. The internal consistency evolves similarly for the four prescriptions: very good internal consistency at small couplings, a rise of the RMSE for larger couplings, and a decrease for very larger couplings. The RMSE decreases in the order: N > S > T > A, implying that velocity reversal after each forbidden hop gives the best performance. The large discrepancy for larger coupling values is not related to the reversal procedure but due to limitations of the decoherence correction used as we discuss below.

The trend in the RMSE can be rationalized as follows. At small coupling values, one can distinguish two domains: around the crossing region (diabatic energy gap $\Delta E = 0$) and around the potential energy minima ($\Delta E = \lambda$). When a peak in the NACE occurs in the crossing region, the time dependent Schrödinger equation transfers electronic population between states and a hop is attempted. As the gap between the adiabatic states is smaller than the thermal energy (see Sec. II B),

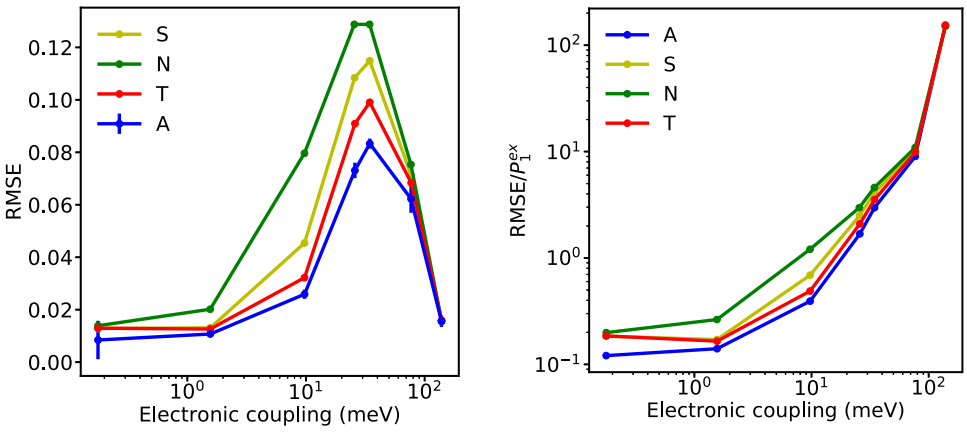

FIG. 4. Influence of the reversing prescription after a rejected hop: (a) root-mean-square error (RMSE) for the internal consistency [Eq. (35)] and (b) relative (RMSE) for different diabatic electronic couplings. "A" means velocities along the direction of the NACVs are always reversed, "T" means they are reversed if Eq. (29) holds, "S" means they are reversed if both Eqs. (29) and (30) hold, and "N" means they are never reversed. Error bars are shown for our default option ("A") and represent standard deviations over five independent blocks of 200 trajectories.

all attempted hops succeed and the internal consistency holds. Away from that region, the decoherence correction Eq. (32) damps the electronic wavefunction to the active state. Both domains concur to maintain a good internal consistency. At larger couplings, between 1 meV and 50 meV, when the energy gap between states becomes larger, the finite value of the NACE in this regime still transfers electronic population between states, but more hops become energy-forbidden. As a result, the electronic population becomes significantly larger than the surface population in this regime as the decoherence term Eq. (31) fails to counteract the electronic population transfer. For very large couplings, the situation improves as the decoherence time decreases [inversely proportional to the energy gap, Eq. (32)], but a significant discrepancy still remains, especially when considering the normalised error in Fig. 4(b). Clearly, an improved description of decoherence is desirable in this regime.

Our analysis of the effect of reversing the velocities after a rejected hop complements previous studies.[48–50,72,73] Since the original work of Tully—which prescribes to always reverse the velocities—different conclusions were obtained for different systems: (i) Müller and Stock[72] obtained better results for the nuclear dynamics of different small model systems without velocity reversal; (ii) Truhlar and co-workers[48,49] explained that reversal of the velocities following Eq. (29) is useful to improve their agreement with more exact quantum calculation; (iii) Jain and Subotnik[50] showed that a small number of reversal events is required to calculate thermal rate correctly using the augmented-FSSH (A-FSSH) method; and (iv) Sifain *et al.*[73] showed that (always) reversing the velocities can slightly improve the detailed balance in two- and three-level systems in contact with a bath. Sifain *et al.*[73] indicated also that the number of frustrated hops decreases when we reverse the velocities that may explain the better internal consistency obtained in our system. If no overall picture emerges about the role of velocity reversal, the three studies carried out for thermal systems (Jain and Subotnik, Sifain *et al.*, and the present work) indicate that reversal of velocities improves the thermal rate, detailed balance, and internal consistency.

V. CONCLUSION

In this work, we have presented significant improvements to the fragment orbital-based surface hopping (FOB-SH) methodology.[24] We have derived an exact expression for the NACVs between the adiabatic electronic states in terms of localized (diabatic) electronic states that we use for the construction of the electronic Hamiltonian. While the final expression for the NACV is quite involved, a numerical analysis of the different contributions shows that the more expensive terms can be safely neglected. The derivation provided is generally applicable to any electronic structure approach where the electronic Hamiltonian is constructed in a localized or diabatic electronic state basis (e.g., sub-system DFT, frozen density embedding,[30] and DFTB[13,14]). This advance permits us to adjust velocities upon successful or frustrated surface hops as suggested in Refs. 41, 48, and 50. Moreover, the NACVs are often required in other non-adiabatic molecular dynamics methods, e.g., in the classical limit of exact factorization approach,[5–7] which may be combined with our FOB scheme in future studies.

Besides NACVs, we have also implemented simple correction schemes for two well-known problems of FSSH: the energy-based decoherence correction (EDC) of Truhlar and co-workers[53,56] to address the overcoherence of the electronic wavefunction and the self-consistent FSSH scheme of Wang and Prezhdo for detection of trivial crossings.[65] The latter are problematic especially for charge transport simulations in large systems where electronic states are sometimes only very weakly coupled. To assess the performance of these modifications to the original FSSH method, we considered three desirable properties of surface hopping simulation: energy conservation, detailed balance, and internal consistency.

Total energy conservation along a SH trajectory is usually impaired by the frequent force discontinuities that the nuclei experience due to hops between electronic surfaces and due to cusps on the active electronic surface. Only the latter issue can be addressed by using small enough time steps. Therefore, total energy drift in FSSH will always be higher than in MD simulations on a single electronic state. We have shown that the total energy conservation of our FOB-SH scheme is reasonably good and improves with decreasing time increments indicating that the nuclear forces are correctly implemented. The self-consistent FSSH scheme is very beneficial in this respect allowing us to use 5 times larger nuclear time steps at a comparable total energy drift.

Detailed balance is a long-standing issue in surface hopping simulations. Tully and co-workers showed for a simple model system that FSSH should reach detailed balance in the limit of small adiabatic energy gaps and/or large NACVs, but only qualitative arguments were given that detailed balance may be satisfied also for larger energy gaps.[34,42] We have shown for a simple molecular ET reaction between two ethylene-like molecules that FOB-SH satisfies detailed balance for a large range of energy gaps and populations spanning four orders of magnitudes. We would like to emphasize that it proved absolutely vital to adjust the velocities along the NACV to determine whether a hop is energy-allowed. If the total kinetic energy is used instead, the population of the excited state is vastly overestimated as soon as the adiabatic energy gap ($2H_{ab}$ at an avoided crossing) exceeds about $k_{\mathrm{B}}T/2$, that is, the average kinetic energy along the NACV. This is typically the case for simulations of charge transfer in organic materials or DNA. In this regime, the incorporation of energy-forbidden hops is essential to obtain detailed balance and this is not possible if the total kinetic energy is taken. That the total kinetic energy should not be used as an energy-criterion becomes obvious if one recalls that this is a size-extensive quantity and that the excited state population of, e.g., a solvated molecule should not depend on the size of the solvent subsystem.

Finally, we have quantified the internal consistency between average surface population and average electronic amplitudes in our simulations and we have compared the effect of different velocity reversing prescriptions. We found that for small adiabatic energy gaps (small diabatic couplings), FOB-SH is internally consistent, with deviations between the averages of only about 10%-20%. However, as the adiabatic

energy gap/diabatic coupling increases, the average electronic amplitude of the excited state becomes strongly overestimated, even when using the EDC decoherence correction. Reversing the velocity along the direction of the NACV after each rejected hop (as suggested by Tully) slightly improves the situation but the remaining inconsistency is still large. The reason is that in this regime an increasing number of hops to excited states are energy-forbidden as required to satisfy detailed balance. By contrast, the NACE between these states are finite, albeit small, giving rise to transfer of population to excited states which is not sufficiently damped by the EDC decoherence correction.

In future works, we intend to investigate how to amend the electronic propagation, using for instance alternative decoherence correction schemes or a modified time-dependent Schrödinger equation as suggested by Fang and Hammes-Schiffer.[52] Including these further improvements, the FOB-SH method is poised to become an efficient method for realistic simulation of charge carrier dynamics in materials science and biology.

ACKNOWLEDGMENTS

A.C. and S.G. were supported by the European Research Council (ERC) under the European Unions Horizon 2020 research and innovation programme (Grant Agreement No. 682539/SOFTCHARGE). Via our membership of the UK's HEC Materials Chemistry Consortium, which is funded by EPSRC (EP/L000202), this work used the ARCHER UK National Supercomputing Service (http://www.archer.ac.uk).

APPENDIX A: NACV BETWEEN ADIABATS FROM NUCLEAR GRADIENTS OF DIABATS

1. Derivation of Eq. (10)

The derivation of the NACV and the nuclear forces starts from the following relationship. Using the chain rule, we write

$$\nabla_I\langle\psi_i|H|\psi_j\rangle = \langle\nabla_I\psi_i|H|\psi_j\rangle + \langle\psi_i|\nabla_I H|\psi_j\rangle + \langle\psi_i|H|\nabla_I\psi_j\rangle\ . \tag{A1}$$

Since the $|\psi_i\rangle$ are the eigenvectors of H, the equation simplifies as

$$\nabla_I E_j\delta_{ij} = E_j\langle\nabla_I\psi_i|\psi_j\rangle + \langle\psi_i|\nabla_I H|\psi_j\rangle + E_i\langle\psi_i|\nabla_I\psi_j\rangle\ . \tag{A2}$$

Applying this equation separately for the diagonal element ($i=j$) and the off-diagonal element ($i\neq j$) and using the definition of nuclear forces ($\boldsymbol{F}_I = -\nabla_I\langle\psi_i|H|\psi_i\rangle$) along with the definition of NACV ($\mathbf{d}^{\mathrm{ad}}_{I,ij} = \langle\psi_i|\nabla_I\psi_j\rangle$), we obtain the second equality in Eq. (6) (i.e., the Hellmann-Feynman theorem) and Eq. (10).

2. Derivation of Eqs. (14)–(16)

Both expressions for the NACV and the forces contain the matrix element of the gradient of the Hamiltonian $\langle\psi_i|\nabla_I H|\psi_j\rangle$. To express this quantity in terms of nuclear gradients in the diabatic basis we insert the transformation Eq. (8) to obtain

$$\langle\psi_i|\nabla_I H|\psi_j\rangle = [\mathbb{U}^\dagger\mathbb{G}_I\mathbb{U}]_{ij}, \tag{A3}$$

where $[\mathbb{G}_I]_{kl} = \langle\phi_k|\nabla_I H|\phi_l\rangle$. Some algebraic modifications give

$$\begin{aligned}
[\mathbb{G}_I]_{kl} &= \langle\phi_k|\nabla_I H|\phi_l\rangle \\
&= \nabla_I\langle\phi_k|H|\phi_l\rangle - \langle\nabla_I\phi_k|H|\phi_l\rangle - \langle\phi_k|H|\nabla_I\phi_l\rangle && \text{(A4)}\\
&= \nabla_I H_{kl} - \langle\nabla_I\phi_k|\sum_m H_{ml}\phi_m\rangle - \langle\nabla_I\phi_l|\sum_m H_{mk}\phi_m\rangle* && \text{(A5)}\\
&= \nabla_I H_{kl} + \left(\sum_m [\mathbb{D}_I]_{km}H_{ml} - H_{km}[\mathbb{D}_I]_{ml}\right) && \text{(A6)}\\
&= \nabla_I H_{kl} + [\mathbb{D}_I, \mathbb{H}]_{kl}, && \text{(A7)}
\end{aligned}$$

where $[\mathbb{D}_I]_{kl} = \langle\phi_k|\nabla_I\phi_l\rangle$ are the NACV in the diabatic basis set and $[\ldots,\ldots\ ]$ indicates the commutator in the last equation. As $\mathbb{U}$ is the unitary transformation that diagonalizes $\mathbb{H}$, such matrix converts the commutator simply as follows:

$$[\mathbb{U}^\dagger[\mathbb{D}_I, \mathbb{H}]\mathbb{U}]_{ij} = [\mathbb{U}^\dagger\mathbb{D}_I\mathbb{U}]_{ij}(E_j - E_i). \tag{A8}$$

Insertion of Eqs. (A7) and (A8) in Eq. (A3) gives for $i=j$ and $i\neq j$, respectively,

$$\langle\psi_i|\nabla_I H|\psi_i\rangle = [\mathbb{U}^\dagger\nabla_I\mathbb{H}\mathbb{U}]_{ii}, \tag{A9}$$

$$\langle\psi_i|\nabla_I H|\psi_j\rangle = [\mathbb{U}^\dagger\nabla_I\mathbb{H}\mathbb{U}]_{ij} + [\mathbb{U}^\dagger\mathbb{D}_I\mathbb{U}]_{ij}(E_j - E_i)\ , \tag{A10}$$

which demonstrates the third equality in Eq. (6) and Eqs. (14)–(16).

3. Derivation of Eq. (17)

According to Eq. (A9) the NACVs in the orthogonal diabatic basis, $\mathbb{D}_I$ are required to obtain the adiabatic NACVs. As the NACVs are calculated numerically between the non-orthogonal diabatic states (giving $\mathbb{D}'_I$), we use Eq. (2) to express $\mathbb{D}_I$ in terms of $\mathbb{D}'_I$

$$\begin{aligned}
[\mathbb{D}_I]_{kl} &= \langle\phi_k|\nabla_I\phi_l\rangle && \text{(A11)}\\
&= \sum_m T_{mk}\langle\varphi_m|\nabla_I\left(\sum_n T_{nl}|\varphi_n\rangle\right) && \text{(A12)}\\
&= \sum_{m,n} T_{mk}\langle\varphi_m|\nabla_I|\varphi_n\rangle T_{nl} + \sum_{m,n} T_{mk}\langle\varphi_m|\varphi_n\rangle\nabla_I T_{nl} && \text{(A13)}\\
&= [\mathbb{T}^\dagger\mathbb{D}'_I\mathbb{T}]_{kl} + [\mathbb{T}^\dagger\mathbb{S}\nabla_I\mathbb{T}]_{kl} && \text{(A14)}\\
&= [\mathbb{T}\mathbb{D}'_I\mathbb{T}]_{kl} + [\mathbb{T}^{-1}\nabla_I\mathbb{T}]_{kl}, && \text{(A15)}
\end{aligned}$$

where

$$[\mathbb{D}'_I]_{mn} = \langle\varphi_m|\nabla_I\varphi_n\rangle\ . \tag{A16}$$

In Eq. (A13) we have used the fact that $\mathbb{T}$ is hermitic ($\mathbb{T} = \mathbb{T}^\dagger$) and that $\mathbb{T} = \mathbb{S}^{-1/2}$. Equation (A15) is identical with Eq. (17) in the main text.

4. Derivation of Eq. (20)

The last term in Eq. (A15) involves the gradient of the Löwdin transformation $\nabla_I\mathbb{T}$. To express this gradient in terms of the gradient of the overlap matrix, which is calculated numerically in our scheme, one proceeds in two steps. First, one relates the gradient of $\mathbb{T} = \mathbb{S}^{-1/2}$ to the one of $\mathbb{S}^{-1}$ with

$$\mathbb{S}^{-1} = \mathbb{S}^{-1/2}\mathbb{S}^{-1/2}, \tag{A17}$$

$$\nabla_I\mathbb{S}^{-1} = \nabla_I\mathbb{S}^{-1/2}\mathbb{S}^{-1/2} + \mathbb{S}^{-1/2}\nabla_I\mathbb{S}^{-1/2}. \tag{A18}$$

We now define the transformation matrix $\mathbb{L}$ that diagonalizes $\mathbb{T}$ and the diagonal matrix $\mathbb{T}^{diag}$ with $\mathbb{T} = \mathbb{S}^{-1/2} = \mathbb{L}\mathbb{T}^{diag}\mathbb{L}^\dagger$. Using this expression and Eq. (A18), one obtains

$$\mathbb{L}^\dagger\nabla_I\mathbb{S}^{-1}\mathbb{L} = \mathbb{L}^\dagger\nabla_I\mathbb{S}^{-1/2}\mathbb{L}\mathbb{T}^{diag} + \mathbb{T}^{diag}\mathbb{L}^\dagger\nabla_I\mathbb{S}^{-1/2}\mathbb{L}, \tag{A19}$$

$$\mathbb{L}^\dagger\nabla_I\mathbb{S}^{-1}\mathbb{L} = \mathbb{W}_I\mathbb{T}^{diag} + \mathbb{T}^{diag}\mathbb{W}_I, \tag{A20}$$

$$[\mathbb{L}^\dagger\nabla_I\mathbb{S}^{-1}\mathbb{L}]_{kl} = [\mathbb{W}_I]_{kl}[\mathbb{T}^{diag}]_{ll} + [\mathbb{T}^{diag}]_{kk}[\mathbb{W}_I]_{kl}, \tag{A21}$$

where we define $\mathbb{W}_I = \mathbb{L}^\dagger\nabla_I\mathbb{S}^{-1/2}\mathbb{L}$. We thus obtain

$$\nabla_I\mathbb{S}^{-1/2} = \mathbb{L}\mathbb{W}_I\mathbb{L}^\dagger \tag{A22}$$

with matrix elements $[\mathbb{W}_I]_{kl}$ obtained from Eq. (A21),

$$[\mathbb{W}_I]_{kl} = \frac{1}{[\mathbb{T}^{diag}]_{kk} + [\mathbb{T}^{diag}]_{ll}}[\mathbb{L}^\dagger\nabla_I\mathbb{S}^{-1}\mathbb{L}]_{kl}. \tag{A23}$$

Secondly, $\nabla_I\mathbb{S}^{-1}$ can be related to $\nabla_I\mathbb{S}$. Starting from $\mathbb{S}^{-1} = \mathbb{S}^{-1}\mathbb{S}\mathbb{S}^{-1}$, one can easily show that: $\nabla_I\mathbb{S}^{-1} = -\mathbb{S}^{-1}(\nabla_I\mathbb{S})\mathbb{S}^{-1}$. We can now express $\mathbb{W}_I$ in terms of $\nabla_I\mathbb{S}$,

$$\begin{aligned}
\nabla_I\mathbb{S}^{-1/2} &= \mathbb{L}\mathbb{W}_I\mathbb{L}^\dagger,\\
[\mathbb{W}_I]_{kl} &= -\frac{1}{[\mathbb{T}^{diag}]_{kk} + [\mathbb{T}^{diag}]_{ll}}[\mathbb{L}^\dagger\mathbb{S}^{-1}(\nabla_I\mathbb{S})\mathbb{S}^{-1}\mathbb{L}]_{kl}\\
&= -\frac{1}{[\mathbb{T}^{diag}]_{kk} + [\mathbb{T}^{diag}]_{ll}}[(\mathbb{T}^{diag})^2\mathbb{L}^\dagger(\nabla_I\mathbb{S})\mathbb{L}(\mathbb{T}^{diag})^2)]_{kl}\\
&= -\frac{([\mathbb{T}^{diag}]_{kk})^2([\mathbb{T}^{diag}]_{ll})^2}{[\mathbb{T}^{diag}]_{kk} + [\mathbb{T}^{diag}]_{ll}}[\mathbb{L}^\dagger(\nabla_I\mathbb{S})\mathbb{L}]_{kl},
\end{aligned} \tag{A24}$$

where we have inserted $\mathbb{S}^{-1} = \mathbb{T}^2 = \mathbb{L}(\mathbb{T}^{diag})^2\mathbb{L}^\dagger$ in Eq. (A24). Finally, the last term of Eq. (A15) reads

$$\begin{aligned}
\mathbb{T}^{-1}\nabla_I\mathbb{T} &= \mathbb{T}^{-1}\nabla_I\mathbb{S}^{-1/2}\\
&= \mathbb{T}^{-1}\mathbb{L}\mathbb{W}_I\mathbb{L}^\dagger\\
&= \mathbb{L}\mathbb{W}'_I\mathbb{L}^\dagger,
\end{aligned} \tag{A25}$$

with

$$\begin{aligned}
[\mathbb{W}'_I]_{kl} &= [(\mathbb{T}^{diag})^{-1}\mathbb{W}_I]_{kl}\\
&= ([\mathbb{T}^{diag}]_{kk})^{-1}[\mathbb{W}_I]_{kl}\\
&= -\frac{[\mathbb{T}^{diag}]_{kk}([\mathbb{T}^{diag}]_{ll})^2}{[\mathbb{T}^{diag}]_{kk} + [\mathbb{T}^{diag}]_{ll}}[\mathbb{L}^\dagger(\nabla_I\mathbb{S})\mathbb{L}]_{kl}
\end{aligned} \tag{A26}$$

Equation (A25) proves the second term of Eq. (20) and Eq. (A26) is identical with Eq. (21) in the main text. This concludes the derivation of the adiabatic NACV within the FOB-SH framework.

APPENDIX B: THERMAL ENERGY ALONG THE NACV DIRECTION

We calculate here the average value of $B^2/4A$, where

$$A = \sum_I \frac{1}{2M_I}|\mathbf{d}^{\mathrm{ad}}_{I,an}|^2\,,$$

$$B = \sum_I \dot{\mathbf{R}}_I \cdot \mathbf{d}^{\mathrm{ad}}_{I,an}.$$

Its derivation reads

$$\begin{aligned}
\left\langle\frac{B^2}{4A}\right\rangle &= \left\langle\frac{1}{4A}\left(\sum_I \dot{\mathbf{R}}_I\cdot\mathbf{d}^{\mathrm{ad}}_{I,an}\right)^2\right\rangle\\
&= \sum_I\sum_J\sum_\alpha\sum_\beta\left\langle\frac{d^{\mathrm{ad},\alpha}_{I,an}d^{\mathrm{ad},\beta}_{J,an}}{4A}\dot{R}_{I,\alpha}\dot{R}_{J,\beta}\right\rangle\\
&= \sum_I\sum_J\sum_\alpha\sum_\beta\left\langle\frac{d^{\mathrm{ad},\alpha}_{I,an}d^{\mathrm{ad},\beta}_{J,an}}{4A}\right\rangle\left\langle\dot{R}_{I,\alpha}\dot{R}_{J,\beta}\right\rangle\\
&= \sum_I\sum_J\sum_\alpha\sum_\beta\left\langle\frac{d^{\mathrm{ad},\alpha}_{I,an}d^{\mathrm{ad},\beta}_{J,an}}{4A}\right\rangle\frac{k_BT}{M_I}\delta_{I,J}\delta_{\alpha,\beta}\\
&= k_BT\left\langle\frac{1}{4A}\sum_I\frac{|\mathbf{d}^{\mathrm{ad}}_{I,an}|^2}{M_I}\right\rangle\\
&= k_BT\left\langle\frac{1}{4A}2A\right\rangle\\
&= \frac{k_BT}{2}.
\end{aligned}$$

APPENDIX C: APPROXIMATION OF NACV BETWEEN DETERMINANTS BY NACV BETWEEN ORBITALS

In the following, we consider a system composed of a donor (D) and an acceptor molecule (A) with total electron number $2N$. We add an extra electron to the system and assume that in the initial ET state "a" the electron is localized on the donor and in the final ET state "b" on the acceptor. We further assert that the initial and final state diabatic wavefunctions are well described by a single determinant, as obtained, for instance, from charge constrained DFT (CDFT),

$$\Phi_\mathrm{a} = \frac{1}{\sqrt{(2N+1)!}}\det(\varphi^1_\mathrm{a}\cdots\varphi^{2N}_\mathrm{a}\varphi^{2N+1}_\mathrm{a}), \tag{C1}$$

$$\Phi_\mathrm{b} = \frac{1}{\sqrt{(2N+1)!}}\det(\varphi^1_\mathrm{b}\cdots\varphi^{2N}_\mathrm{b}\varphi^{2N+1}_\mathrm{b}). \tag{C2}$$

The orbitals forming a determinant are assumed to be orthogonal, $\langle\varphi^i_\mathrm{a}|\varphi^j_\mathrm{a}\rangle = \delta_{ij}$, but orbitals of different determinants are in general not orthogonal. Calculation of the NACV involves taking the nuclear gradient of the wavefunction. For instance, the derivative with respect to the x-component of nucleus I can be written as follows:

$$\begin{aligned}
\langle\Phi_\mathrm{a}|\frac{\partial}{\partial R_{I,x}}\Phi_\mathrm{b}\rangle = \frac{1}{\epsilon}\frac{1}{(2N+1)!}\Big(&\Big\langle\det\left(\varphi^1_\mathrm{a}\cdots\varphi^{2N}_\mathrm{a}\varphi^{2N+1}_\mathrm{a}\right)\\
&\times\left|\det(\tilde{\varphi}^1_\mathrm{b}\cdots\tilde{\varphi}^{2N}_\mathrm{b}\tilde{\varphi}^{2N+1}_\mathrm{b})\right\rangle\\
&-\left\langle\det\left(\varphi^1_\mathrm{a}\cdots\varphi^{2N}_\mathrm{a}\varphi^{2N+1}_\mathrm{a}\right)\right.\\
&\times\left.\left|\det\left(\varphi^1_\mathrm{b}\cdots\varphi^{2N}_\mathrm{b}\varphi^{2N+1}_\mathrm{b}\right)\right\rangle\right),
\end{aligned} \tag{C3}$$

where $\tilde{\varphi}^i_\mathrm{b}$, $i = 1, \ldots, 2N+1$ are the perturbed orbitals obtained after a small displacement of nucleus I along the x-direction, $\tilde{\varphi}^i_\mathrm{b} = \varphi^i_\mathrm{b}(\mathbf{R}_1, \ldots, \mathbf{R}_I + \epsilon\mathbf{e}_{I,x}, \ldots, \mathbf{R}_M)$, with $\boldsymbol{e}_{I,x}$ the unit vector in the x-direction. The perturbed orbitals can be obtained, e.g., from CDFT calculations on the perturbed structure.

Now we would like to analyse under which conditions the NACV component between the charge transfer determinants Φ_a and Φ_b, Eq. (C3), can be approximated by the NACV component between the HOMOs in the two CT states,

$$\left\langle \varphi_a^{2N+1} \middle| \frac{\partial}{\partial R_{I,x}} \varphi_b^{2N+1} \right\rangle = \frac{1}{\epsilon} \left(\left\langle \varphi_a^{2N+1} \middle| \tilde{\varphi}_b^{2N+1} \right\rangle - \left\langle \varphi_a^{2N+1} \middle| \varphi_b^{2N+1} \right\rangle \right). \tag{C4}$$

In a first approximation, we assume that the orbitals 1 to $2N$ remain unchanged (frozen) as the excess electron moves from the donor to the acceptor,

$$\varphi_a^i = \varphi_b^i \quad \forall i = 1, \ldots, 2N. \tag{C5}$$

As the orbitals within a determinant are assumed to be orthogonal, we obtain for the second term on the RHS of Eq. (C3)

$$\frac{1}{(2N+1)!} \langle \det(\varphi_a^1 \cdots \varphi_a^{2N} \varphi_a^{2N+1}) | \det(\varphi_b^1 \cdots \varphi_b^{2N} \varphi_b^{2N+1}) \rangle = \langle \varphi_a^{2N+1} | \varphi_b^{2N+1} \rangle. \tag{C6}$$

In a second approximation, we assume that the perturbation is small so that the perturbed orbitals in state b remain orthonormal to the ones in state a,

$$\langle \varphi_a^i | \tilde{\varphi}_b^j \rangle = \delta_{ij} \quad \forall i = 1, \ldots, 2N, \forall j = 1, \ldots, 2N+1. \tag{C7}$$

In this case, the first term on the RHS of Eq. (C3) simplifies to

$$\frac{1}{(2N+1)!} \langle \det(\varphi_a^1 \cdots \varphi_a^{2N} \varphi_a^{2N+1}) | \det(\tilde{\varphi}_b^1 \cdots \tilde{\varphi}_b^{2N} \tilde{\varphi}_b^{2N+1}) = \langle \varphi_a^{2N+1} | \tilde{\varphi}_b^{2N+1} \rangle. \tag{C8}$$

Insertion of Eqs. (C6) and (C8) in Eq. (C3) and using Eq. (C4), we find

$$\left\langle \Phi_a \middle| \frac{\partial}{\partial R_{I,x}} \Phi_b \right\rangle = \left\langle \varphi_a^{2N+1} \middle| \frac{\partial}{\partial R_{I,x}} \varphi_b^{2N+1} \right\rangle. \tag{C9}$$

Hence, for Eq. (C9) to hold, Eqs. (C5) and (C7) must be assumed. We note that the approximation Eq. (C5) is also made in fragment-orbital DFT (FODFT) calculation of electronic coupling matrix elements between donor and acceptor[74,75] resulting in a relatively small error for couplings when compared to *ab initio* benchmark data.[76,77] The same should be true for the overlap Eq. (C6) as the latter is approximately proportional to electronic coupling. It is less clear how well approximation Eq. (C7) is fulfilled. In practice, the overlap between the perturbed orbital $\tilde{\varphi}_b^i$ and φ_a^i will be smaller than one, and similarly $\tilde{\varphi}_b^i$ will not stay fully orthonormal to the other orbitals φ_a^j, $j \neq i$. One can expect that these effects are likely to cancel one another to some extent.

[1] G. A. Worth, H.-D. Meyer, H. Koäppel, L. S. Cederbaum, and I. Burghardt, Int. Rev. Phys. Chem. **27**, 569 (2008).
[2] H. Tamura and I. Burghardt, J. Am. Chem. Soc. **135**, 16364 (2013).
[3] T. J. Martinez, M. Ben-Nun, and R. Levine, J. Chem. Phys. **100**, 7884 (1996).
[4] T. J. Martinez, Acc. Chem. Res. **39**, 119 (2006).
[5] A. Abedi, N. T. Maitra, and E. K. U. Gross, Phys. Rev. Lett. **105**, 123002 (2010).
[6] A. Abedi, N. T. Maitra, and E. K. U. Gross, J. Chem. Phys. **137**, 22A530 (2012).
[7] F. Agostini, A. Abedi, and E. K. U. Gross, J. Chem. Phys. **141**, 214101 (2014).
[8] P. Ehrenfest, Z. Phys. **45**, 455–457 (1927).
[9] J. C. Tully, J. Chem. Phys. **93**, 1061 (1990).
[10] M. Elstner, D. Porezag, G. Jungnickel, J. Elsner, M. Haugk, T. Frauenheim, S. Suhai, and G. Seifert, Phys. Rev. B **58**, 7260 (1998).
[11] T. A. Niehaus, D. Heringer, B. Torralva, and T. Frauenheim, Eur. Phys. J. D **35**, 467 (2005).
[12] T. Kubař, U. Kleinekathoäfer, and M. Elstner, J. Phys. Chem. B **113**, 13107 (2009).
[13] T. Kubař and M. Elstner, Phys. Chem. Chem. Phys. **15**, 5794 (2013).
[14] T. Kubař and M. Elstner, J. R. Soc., Interface **10**, 20130415 (2013).
[15] S. Pal, D. J. Trivedi, A. V. Akimov, B. Aradi, T. Frauenheim, and O. V. Prezhdo, J. Chem. Theory Comput. **12**, 1436–1448 (2016).
[16] R. Mitrić, U. Werner, M. Wohlgemuth, G. Seifert, and V. Bonačić-Koutecký, J. Phys. Chem. A **113**, 12700 (2009).
[17] T. Kubař and M. Elstner, J. Phys. Chem. B **114**, 11221 (2010).
[18] E. Fabiano, T. W. Keal, and W. Thiel, Chem. Phys. **349**, 334 (2008).
[19] Z. Lan, E. Fabiano, and W. Thiel, J. Phys. Chem. B **113**, 3548–3555 (2009).
[20] T. Nelson, S. Fernandez-Alberti, V. Chernyak, A. E. Roitberg, and S. Tretiak, J. Phys. Chem. B **115**, 5402–5414 (2011).
[21] T. Nelson, S. Fernandez-Alberti, A. E. Roitberg, and S. Tretiak, Acc. Chem. Res. **47**, 1155–1164 (2014).
[22] F. Sterpone and P. J. Rossky, J. Phys. Chem. B **112**, 4983 (2008).
[23] M. J. Bedard-Hearn, F. Sterpone, and P. J. Rossky, J. Phys. Chem. A **114**, 7661 (2010).
[24] J. Spencer, F. Gajdos, and J. Blumberger, J. Chem. Phys. **145**, 064102 (2016).
[25] Q. Wu and T. Van Voorhis, Phys. Rev. A **72**, 024502 (2005).
[26] Q. Wu, C.-L. Cheng, and T. Van Voorhis, J. Chem. Phys. **127**, 164119 (2007).
[27] H. Oberhofer and J. Blumberger, J. Chem. Phys. **131**, 064101 (2009).
[28] H. Oberhofer and J. Blumberger, J. Chem. Phys. **133**, 244105 (2010).
[29] A. de la Lande and D. R. Salahub, J. Mol. Struct.: THEOCHEM **943**, 115 (2010).
[30] M. Pavanello and J. Neugebauer, J. Chem. Phys. **135**, 234103 (2011).
[31] P. Ramos, M. Papadakis, and M. Pavanello, J. Phys. Chem. B **119**, 7541 (2015).
[32] F. Gajdos, S. Valner, F. Hoffmann, J. Spencer, M. Breuer, A. Kubas, M. Dupuis, and J. Blumberger, J. Chem. Theory Comput. **10**, 4653 (2014).
[33] A. V. Akimov, J. Chem. Theory Comput. **12**, 5719 (2016).
[34] J. R. Schmidt, P. V. Parandekar, and J. C. Tully, J. Chem. Phys. **129**, 044104 (2008).
[35] G. Granucci and M. Persico, J. Chem. Phys. **126**, 134114 (2007).
[36] T. Nelson, S. Fernandez-Alberti, A. E. Roitberg, and S. Tretiak, J. Chem. Phys. **138**, 224111 (2013).
[37] J. Blumberger and K. McKenna, Phys. Chem. Chem. Phys. **15**, 2184 (2013).
[38] G. Granucci, M. Persico, and A. Toniolo, J. Chem. Phys. **114**, 10608 (2001).
[39] F. Plasser, G. Granucci, J. Pittner, M. Barbatti, M. Persico, and H. Lischka, J. Chem. Phys. **137**, 22A514 (2012).
[40] S. Mai, P. Marquetand, and L. González, Int. J. Quantum Chem. **115**, 1215 (2015).
[41] See endnote 39 in S. Hammes-Schiffer and J. C. Tully, J. Chem. Phys. **101**, 4657 (1994).
[42] P. V. Parandekar and J. C. Tully, J. Chem. Phys. **122**, 094102 (2005).
[43] P. Pechukas, Phys. Rev. **181**, 174 (1969).
[44] M. F. Herman, J. Chem. Phys. **81**, 754 (1984).
[45] Y. Wu and M. F. Herman, J. Chem. Phys. **127**, 044109 (2007).
[46] D. F. Coker and L. Xiao, J. Chem. Phys. **102**, 496 (1995).
[47] M. D. Hack, A. W. Jasper, Y. L. Volobuev, D. W. Schwenke, and D. G. Truhlar, J. Phys. Chem. A **103**, 6309 (1999).
[48] A. W. Jasper and D. G. Truhlar, Chem. Phys. Lett. **369**, 60 (2003).
[49] A. W. Jasper, M. D. Hack, and D. G. Truhlar, J. Chem. Phys. **115**, 1804 (2001).
[50] A. Jain and J. E. Subotnik, J. Chem. Phys. **143**, 134107 (2015).
[51] B. J. Schwartz, E. R. Bittner, O. V. Prezhdo, and P. J. Rossky, J. Chem. Phys. **104**, 5942 (1996).
[52] J. Y. Fang and S. Hammes-Schiffer, J. Phys. Chem. A **103**, 9399 (1999).
[53] C. Zhu, S. Nangia, A. W. Jasper, and D. G. Truhlar, J. Chem. Phys. **121**, 7658 (2004).
[54] T. Nelson, S. Fernandez-Alberti, A. E. Roitberg, and S. Tretiak, J. Phys. Chem. Lett. **8**, 3020 (2017).
[55] B. R. Landry and J. E. Subotnik, J. Chem. Phys. **135**, 191101 (2011).
[56] C. Zhu, A. W. Jasper, and D. G. Truhlar, J. Chem. Phys. **120**, 5543 (2004).
[57] B. R. Landry and J. E. Subotnik, J. Chem. Phys. **137**, 22A513 (2012).
[58] M. J. Falk, B. R. Landry, and J. E. Subotnik, J. Phys. Chem. B **118**, 8108 (2014).
[59] G. Granucci, M. Persico, and A. Zoccante, J. Chem. Phys. **133**, 134111 (2010).

[60]T. Nelson, S. Fernandez-Alberti, A. E. Roitberg, and S. Tretiak, Chem. Phys. Lett. **590**, 208 (2013).
[61]P. Hurd, T. Cusati, and M. Persico, J. Comput. Phys. **229**, 2109 (2010).
[62]S. Fernandez-Alberti, A. E. Roitberg, T. Nelson, and S. Tretiak, J. Chem. Phys. **137**, 014512 (2012).
[63]L. Wang and D. Beljonne, J. Phys. Chem. Lett. **4**, 1888 (2013).
[64]G. A. Meek and B. G. Levine, J. Phys. Chem. Lett. **5**, 2351 (2014).
[65]L. Wang and O. V. Prezhdo, J. Phys. Chem. Lett. **5**, 713 (2014).
[66]J. Spencer, L. Scalfi, A. Carof, and J. Blumberger, Faraday Discuss. **195**, 215 (2016).
[67]D. A. Case, T. A. Darden, T. E. Cheatham III, C. L. Simmerling, J. Wang, R. E. Duke, R. Luo, M. Crowley, R. C. Walker, W. Zhang, K. M. Merz, B. Wang, S. Hayik, A. Roitberg, G. Seabra, I. Kolossvary, K. F. Wong, F. Paesani, J. Vanicek, X. Wu, S. R. Brozell, T. Steinbrecher, H. Gohlke, L. Yang, C. Tan, J. Mongan, V. Hornak, G. Cui, D. H. Mathews, M. G. Seetin, C. Sagui, V. Babin, and P. A. Kollman, AMBER 10, University of California, San Francisco (2008).
[68]C. P. Herrero, Phys. Rev. B **65**, 014112 (2001).
[69]S. Nosé, Mol. Phys. **52**, 255 (1984).
[70]S. Nosé, J. Chem. Phys. **81**, 511 (1984).
[71]CP2K Developers Group, http://www.cp2k.org/.
[72]U. Müller and G. Stock, J. Chem. Phys. **107**, 6230 (1997).
[73]A. E. Sifain, L. Wang, and O. V. Prezhdo, J. Chem. Phys. **144**, 211102 (2016).
[74]H. Oberhofer and J. Blumberger, Phys. Chem. Chem. Phys. **14**, 13846 (2012).
[75]H. Oberhofer and J. Blumberger, Angew. Chem., Int. Ed. **49**, 3631 (2010).
[76]A. Kubas, F. Hoffmann, A. Heck, H. Oberhofer, M. Elstner, and J. Blumberger, J. Chem. Phys. **140**, 104105 (2014).
[77]A. Kubas, F. Gajdos, A. Heck, H. Oberhofer, M. Elstner, and J. Blumberger, Phys. Chem. Chem. Phys. **17**, 14342 (2015).